HOSTED BY
ELSEVIER
CrossMark
Available online at www.sciencedirect.com
ScienceDirect
Progress in Natural Science: Materials International 25 (2015) 642–649
Progress in Natural Science Materials International
www.elsevier.com/locate/pnsmi
www.sciencedirect.com

Original Research

Hybrid aqueous capacitors with improved energy/power performance

Jakub Menzel, Krzysztof Fic, Elzbieta Frackowiak*

Poznan University of Technology, Institute of Chemistry and Technical Electrochemistry, Berdychowo 4, 60965 Poznan, Poland

Received 1 November 2015; accepted 30 November 2015
Available online 22 December 2015

Abstract

This work reports on a high-voltage, hybrid capacitor involving two separate redox reactions. Aqueous solutions of $Mg(NO_3)_2$ and KI have been used for negative and positive electrode, respectively. Adjusting pH=2 for electrode (+) with KI solution and modifying $Mg(NO_3)_2$ solution to pH=9 for negative side play a crucial role for a stable long-term operation of capacitor at enhanced voltage. A benefit from such a construction is a pseudocapacitive contribution from hydrogen sorption reaction on the negative electrode and high iodine/iodide activity on the positive electrode, enhancing the energy with no remarkable impact on the power profile. Proposed solution allows a high voltage (1.8 V) to be reached and thereby high power and energy performance (~20 W h/kg at 1 kW/kg) to be obtained. High long-term stability has been confirmed by floating and galvanostatic tests.
© 2015 The Authors. Chinese Materials Research Society. Production and hosting by Elsevier B.V. This is an open access article under the CC BY-NC-ND license (http://creativecommons.org/licenses/by-nc-nd/4.0/).

Keywords: Electrochemical capacitors; High-voltage systems; Hybrid systems; Carbon electrodes; Aqueous systems; Neutral electrolytes

1. Introduction

Electrochemical capacitors are high power devices designed to fill the gap between batteries and electrolytic capacitors. Application of activated carbon electrodes with high surface area significantly improves the energy performance of these devices over classical capacitor design [1,2]. Electrochemical capacitors can be classified into several groups, depending either on the electrolyte used or the electrodes design; thus, one can distinguish water [3–8], organic [9–13] and ionic liquid [14–16] based supercapacitors. On the other hand, if one will look at the electrode configuration [17] there are two groups, i.e. symmetric AC/AC [18,19] and hybrid capacitors [20–25]. Nevertheless, in all of these groups one always struggles in a compromise between power, energy and cycle life of the final device.

The major disadvantage of AC/AC supercapacitors working in aqueous electrolytes is their low maximum operating voltage (~1 V for H_2SO_4 and KOH solutions) which directly limits the energy output of these devices at ca. 5 W h/kg [26]. With the energy density at such a moderate level, water-based devices will always be less attractive than organic ones, reaching 2.7 V and characterized by maximum energy at the level of ca. 20 W h/kg [27]. Hence, an enhancement of operating voltage is required. To list the benefits of aqueous systems, one can mention typical technological aspects such as easier assembly process (no need for inert atmosphere, material purification processes, and expensive drying steps), user safety and environmental friendliness. Another advantage of the aqueous electrolytic solution is remarkably higher conductivity leading to better power performance.

Recently, in pursuit of improving energy in aqueous-based capacitors, the system operating up to 2.2 V in alkali metal sulfate solution has been reported [8]. However, such extremely high voltage value was achieved on gold current collectors that exclude the parasitic effect of corrosion. Recently, a maximum operational voltage of Li_2SO_4-based electrolyte is reported as 1.5 V [28]. Higher voltages lead to water decomposition and current collectors corrosion. Unfortunately, even at 1.5 V the energy output is still lower than for devices operating in organic solutions. On the other hand, high values of capacitor voltage were achieved by involving redox active transition metal oxide and carbon electrodes. Such asymmetric configurations are

*Corresponding author. Tel.: +48 61 665 36 32; fax: +48 61 665 37 91.
E-mail address: elzbieta.frackowiak@put.poznan.pl (E. Frackowiak).
Peer review under responsibility of Chinese Materials Research Society.

http://dx.doi.org/10.1016/j.pnsc.2015.12.001
1002-0071/© 2015 The Authors. Chinese Materials Research Society. Production and hosting by Elsevier B.V. This is an open access article under the CC BY-NC-ND license (http://creativecommons.org/licenses/by-nc-nd/4.0/).

characterized by high energy efficiency and operation in the voltage range from 1.7 V up to 2.4 V in aqueous electrolytes [29–31].

As the energy of capacitor depends on the amount of charge accumulated, another possibility of energy density improvement is an introduction of fast redox reactions originating either from electrolyte solution like halide ions [24,32,33], hydroquinones [34,35] or electrode material with pseudocapacitive effects [36,37]. In such a hybrid configuration, two different charge storage phenomena are combined: an electrostatic on one electrode with significant potential change during charging/discharging whereas redox-couple determines constant potential of the second electrode with only moderate changes when the voltage of the device is extended. Moreover, electrochemical hydrogen storage has to be considered as a source of additional capacitance on negative electrode [38–42]. An advantage of this phenomenon is the shift of the hydrogen evolution potential; it can be exploited to increase the maximum electrochemical window of aqueous-based supercapacitors.

In this work a high voltage hybrid, aqueous capacitor involving two separate redox reactions is presented. The idea of such device was described in our previous report, where KOH and KI electrolytes were used, and system reached 1.6 V [25]. In this construction, the KOH was replaced by $Mg(NO_3)_2$ and KNO_3 served as an electrolyte for the separator soaking. The novelty of our present system is an additional pH change of electrolyte solution to acidic one for the positive side and into alkaline pH on the negative side. The purpose of such a construction is to benefit from hydrogen sorption reaction on the negative electrode and high iodine/iodide activity on the positive electrode. Proposed solution allows a high voltage to be reached and thereby high power and energy performance to be obtained.

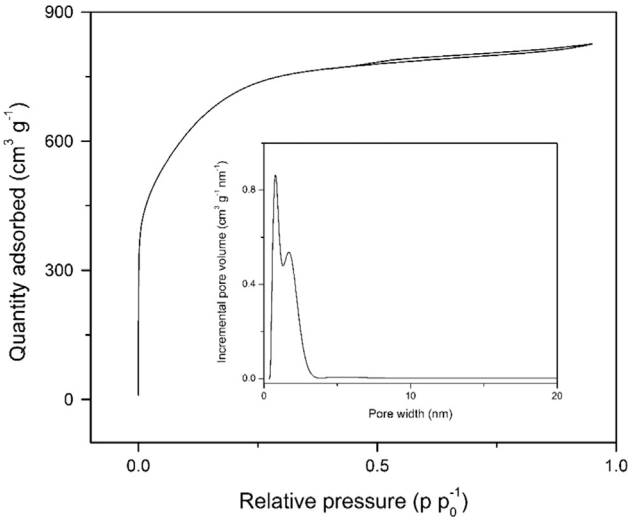

Fig. 1. Nitrogen adsorption/desorption isotherms and pore size distribution of carbon Kuraray® YP80F.

2. Experimental

2.1. Electrode and electrolyte preparation

The electrode material was prepared by mixing of 85 wt% activated carbon AC (Kuraray® YP-80), 10 wt% of poly (tetrafluoroethylene) PTFE (60% water dispersion from Sigma Aldrich®) as a binder and 5 wt% of carbon black (Super C65, Timcal®) used to improve the electrode conductivity. The activated carbon has a typical microporous character and BET specific surface area of ca. 2429 $m^2\ g^{-1}$, measured by nitrogen adsorption/desorption technique at 77 K with ASAP 2460 Micromeritics® (Fig. 1).

Isopropanol was added to electrode components, and the mixture was stirred with heating until all excess of solvent was removed, and homogenous pulp of electrode material was obtained. The material was then calendared to form the self-standing film afterwards. The electrodes for electrochemical investigation were cut in the form of pellets (10 mm diameter, mass 11–13 mg, thickness ca. 0.25 mm). Glass microfibrous Whatman® GF/D filter paper was used as a separator. Electrolytes used were prepared from KNO_3 (99% purity), $Mg(NO_3)_2$•$6H_2O$ (99% purity), KI (> 99% purity), KOH (99% purity) and H_2SO_4 (98% purity); all chemicals were supplied by AVANTOR POLAND®.

For investigation several electrolytes were prepared: 1 M KNO_3, 1 M $Mg(NO_3)_2$, 1 M KI, 1M $Mg(NO_3)_2$/KOH and 1 M KI/H_2SO_4. Mixtures of electrolytes with adjusted pH were made adding drop-by-drop respective 6 M KOH and 0.01 M H_2SO_4 into 1 M solutions with on-line pH control until the desired pH has been obtained. The pH and conductivity of electrolytes were measured by Mettler Tolledo® pH meter and conductivity meter (Table 1).

2.2. Cell configuration

All investigations were performed in two- and three-electrode Swagelok® cell configuration with stainless steel current collectors. The experiments were conducted in two configurations, AC/AC symmetric cells and AC/AC hybrid electrolyte cell. In all cases, firstly the electrodes were immersed in the electrolyte solution and left under vacuum for 1 h. In the case of symmetric cells, both electrodes and separator were immersed in the same electrolyte. In the case of hybrid electrolyte system, the positive electrode was immersed

Table 1
Conductivity and pH of used electrolytes.

	$Mg(NO_3)_2$	KNO_3	KI	$Mg(NO_3)_2$/KOH	KI/H_2SO_4
Conductivity (mS/cm)	111	91	114	111	114
pH	3.4	5.7	5.7	9	2

in KI/H_2SO_4 solution and negative in $Mg(NO_3)_2$/KOH electrolytes. After immersion step, the electrodes were placed on the current collectors and the excess of the electrolyte was removed; in a hybrid configuration, to provide proper separation of specific electrolytes, electrodes were covered by glass fiber separator soaked in 1 M KNO_3 solution.

2.3. Electrochemical measurements

A fundamental electrochemical performance characterization of prepared cells was done by three techniques; galvanostatic charge/discharge with potential limitation (0.5–20 A g^{-1}), cyclic voltammetry (10 mV s^{-1}) and electrochemical impedance spectroscopy (100 kHz–1 mHz). The long-term stability of the systems was tested both by floating technique and galvanostatic charging/discharging at 10 A g^{-1} current density [40].

Three-electrode cell investigation with mercury/mercury sulfate reference electrode (Hg/Hg_2SO_4, $E=0.654$ V vs. NHE) involved galvanostatic charging/discharging at 0.5 A g^{-1} current density to determine the operating potential windows for both electrodes, and afterwards – cyclic voltammetry at 5 mV s^{-1} scan rate. All electrochemical experiments were conducted on multichannel potentiostat/galvanostat VMP3 from BioLogic® France.

3. Results and discussion

3.1. Cyclic voltammetry investigation

Comparison of voltammograms for AC/AC capacitors with mixed $KI/Mg(NO_3)_2$ electrolyte and hybrid separated electrolyte system is shown in Fig. 2. The cells were prepared as described above; before reaching 1.8 V the cells were cycled at 1 V and then the voltage has been increased gradually until 1.8 V with 100 mV stepwise. It has to be noticed that presented profiles are the last cycles of 1.8 V cycling step (for each cell voltage the scanning has been repeated three times). In the case of mixed electrolyte, the average capacitance value is significantly higher (248 F g^{-1}) than for hybrid electrolyte (182 F g^{-1}). Moreover, for a system with mixed electrolytes a deterioration from box-like shape can be observed. At low cell voltages (0–0.3 V) a high current peak appears and the intensity of this response is voltage-dependent. This effect corresponds to the high activity of iodide and iodine species, resulting in the formation of triiodides and polyiodides [35]. Once the voltage of 1.8 V is applied, an additional contribution of hydrogen storage might be observed; we assume that small 'humps' at 1.3 V and 0.3 V might be attributed to hydrogen sorption/desorption process, but the three-electrode experiment is required to confirm this assumption. The increase of the current response at 1.6–1.8 V may correspond to water decomposition processes.

For hybrid electrolyte system (i.e. with KI and $Mg(NO_3)_2$ electrolytes well separated), the typical box-like shape is recorded. However, a negligible increase of current response with voltage increase can be observed, with a small deterioration from a box-like shape at 0.2 V. There are no current peaks at low cell voltages corresponding for high iodine/iodide activity.

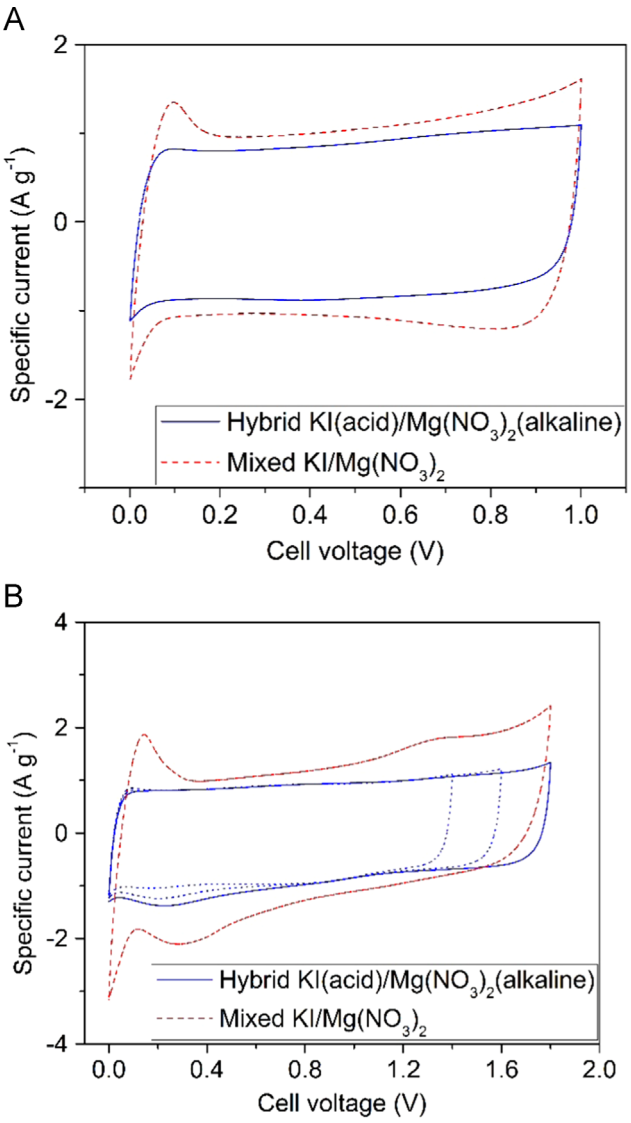

Fig. 2. Voltammograms at 10 mVs^{-1} for hybrid separated electrolyte system and system with mixed electrolytes. (A) cycled to 1 V; (B) gradually cycled to 1.8 V.

Hence, we assume that electrolytes are well separated, and redox activity of iodine is shifted towards higher potential values (to be confirmed by three-electrode investigation). It is worth noting that at 1.8 V one cannot observe a current increase. Hence, it proves that electrochemical capacitor operating in hybrid electrolyte system appears to be stable at 1.8 V (Fig. 2).

3.2. Three-electrode cell investigation

More in-depth study of the aforementioned systems requires a three-electrode investigation. The reference electrode (Hg/Hg_2SO_4 in 0.5 M K_2SO_4, 0.654 mV vs. NHE) has been introduced to the two electrode Swagelok® system. The system was galvanostaticaly charged/discharged at 0.1 A g^{-1} current density to establish the positive and negative electrode potential windows. The result of this experiment is shown in Fig. 3 as the relationship between potentials of electrodes vs. corresponding cell voltage.

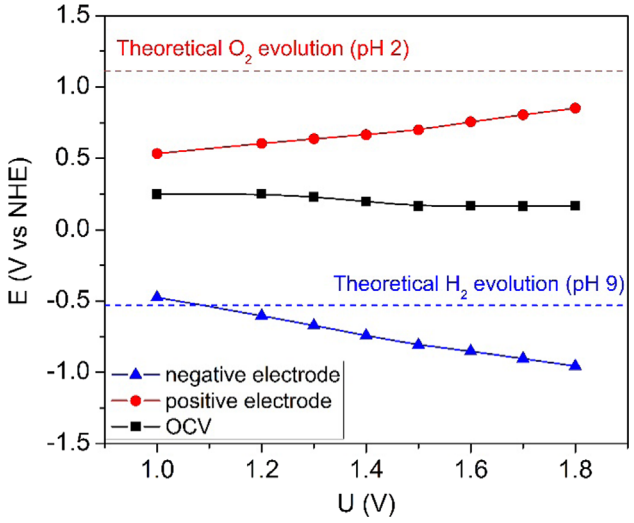

Fig. 3. Potentials vs. NHE of positive and negative electrode vs. voltage of the full cell in hybrid electrolyte system.

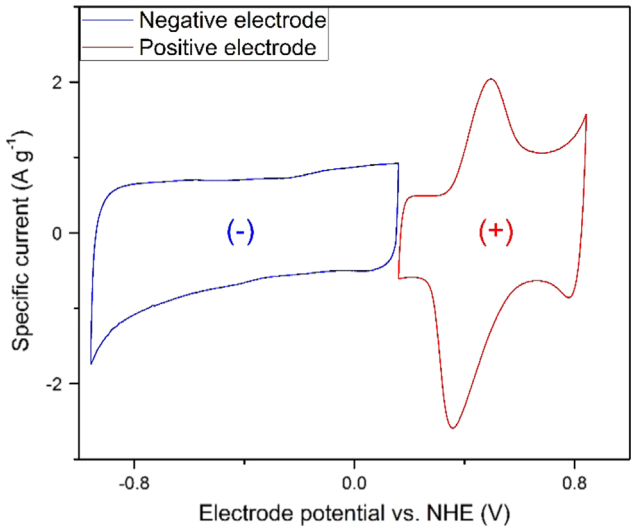

Fig. 4. Voltammograms at 1 mVs^{-1} of negative and positive electrodes vs. NHE for hybrid electrolyte system.

Comparison of obtained voltages with the theoretical potential of O_2 and H_2 evolution for positive and negative electrode confirmed our previous assumptions. The positive electrode potentials reach the values lower than the O_2 evolution limit. Thus, one should not expect gas evolution and decomposition of electrolyte on the positive side. On the other hand, the potential of negative electrode goes deeply above theoretical H_2 evolution limit. In such conditions, one should expect the beneficial pseudocapacitive effect of hydrogen storage and accordingly – increase of capacitance performance of the system. This prediction was confirmed by cyclic voltammetry for individual electrodes, shown in Fig. 4.

The shape of the voltammetry profile suggests that once the potential limit is shifted towards more negative values, hydrogen is stored, and hysteresis loop can be observed. Storage process is followed by desorption process during discharge with corresponding oxidation peak at −0.1 V. Hydrogen storage process can be explained by Volmer reaction; no current perturbation at low potential values excludes Tafel mechanism (hydrogen recombination and evolution). Voltammetry profile for the positive electrode in a potential range corresponding to 1 V of the cell voltage demonstrates typical iodine/iodide redox response [35]. A further shift of maximum potential towards more positive values leads to the formation of the second peak. According to the Pourbaix diagram of iodine, this peak might correspond to the reaction of iodates formation. One should note that IO_3^- specimen is more preferably formed in slightly alkaline solutions, and hydrogen storage process on the negative side might slightly increase a pH of the positive electrode bulk. Finally, the lack of current perturbation and fact that maximum potential value reached is lower than theoretical potential of O_2 evolution, suggest that there is no electrolyte decomposition. Three-electrode cell investigation shows no evidence of gas evolution in the system at potentials corresponding to 1.8 V cell voltage, and confirms the existence of two redox contributions: hydrogen storage on the negative electrode and iodine/iodide/iodate on the positive electrode.

3.3. Floating test and cycle stability performance

The next step of the investigation was focused on the long-term stability of the systems. Two different techniques were involved in this investigation: floating (voltage hold) and galvanostatic cycling [43]. Fig. 5 and Fig. 6 show the comparison of floating results for a system with mixed electrolytes and hybrid electrolyte system. One loop of floating test accounts for 2 hours of voltage hold followed by 50 cycles of galvanostatic charge/discharge at 1 A g^{-1} current density.

For a system with mixed electrolytes, an increase of capacitance value at first several hours of floating test can be observed. This increase of capacitance value originates from the formation, dissolution and reactions between different forms of iodides and iodine demonstrating high redox activity in this region. After several hours of floating a dramatic loss of capacitance might be observed (more than 80% of the initial value of capacitance). A comparison of galvanostatic charge/discharge before and after floating demonstrates an enormous increase of internal resistance in the form of an ohmic drop. This evidence confirms the system failure. Additionally, after measurements, the device was dismounted, and remarkable traces of corrosion were observed.

For the hybrid electrolyte system, good capacitance stability was observed during 60 h of floating. The capacitance retention is maintained at 95%. Moreover, there is no significant difference between galvanostatic charge/discharge profiles recorded before and after the floating test.

The stability of hybrid electrolyte system was also confirmed by 20 000 galvanostatic charging/discharging cycles at 10 A g^{-1} current density. Meanwhile, after each 1 000 cycles, a 1 cycle at 1 A g^{-1} current density has been recorded to monitor the redox-originating changes in the system. A slow decay of capacitance values with cycles was observed. The capacitance retention is 97% of the initial value. Comparison of the first and last cycle at 10 A g^{-1} current density reflects a small resistance increase and improvement of efficiency of the

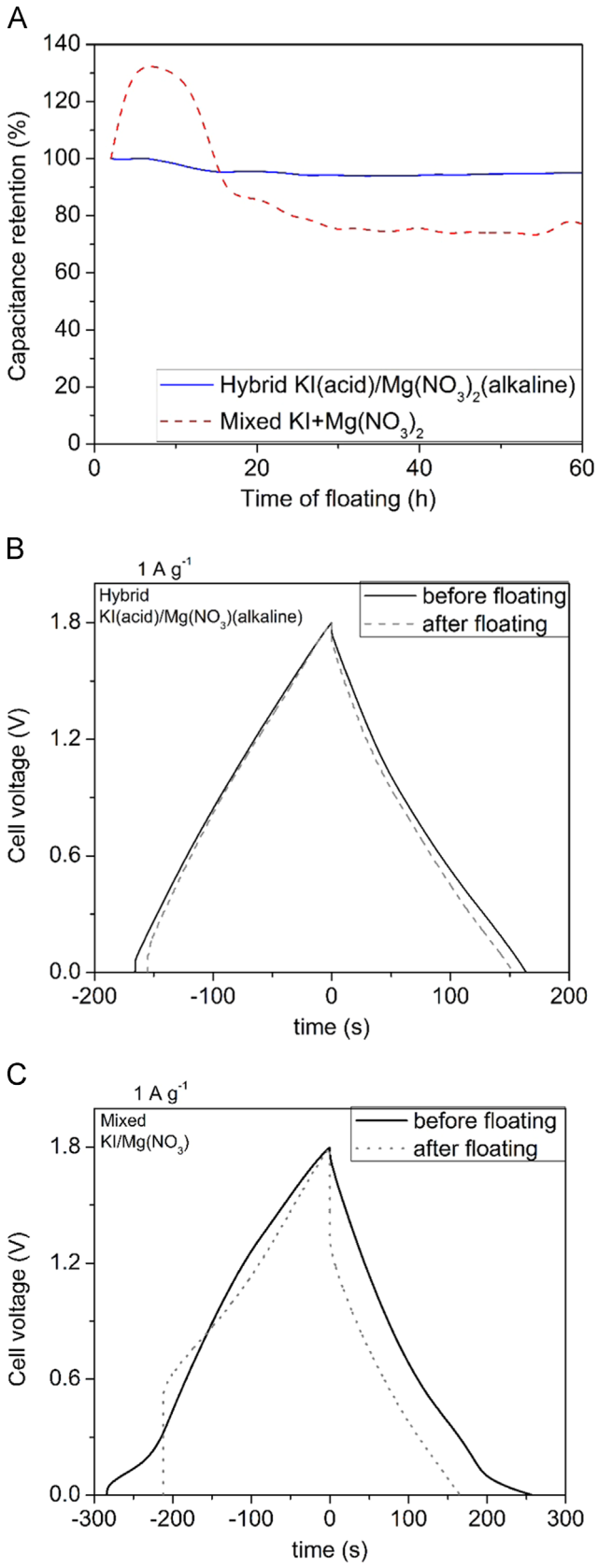

Fig. 5. Capacitance retention recorded during floating test (A) and profiles of charge/discharge before and after floating test for a system with hybrid (B) and mixed (C) electrolyte.

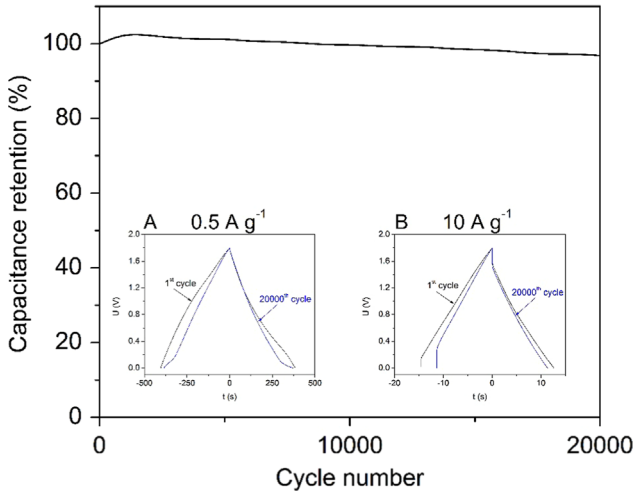

Fig. 6. Capacitance retention recorded for the hybrid system during cycle stability test at 10 Ag^{-1} current density and profiles of charge/discharge after and before the cycle performance test for 0.5 Ag^{-1} (A) and 10 Ag^{-1} current regime (B).

process. The increase in resistance of the cell is probably not connected with electrochemical nature of the system but rather with the imperfection of test system, demonstrated by EIS experiment and discussed later. However, during fast charge/discharge no significant contribution of hydrogen storage was observed, the comparison of low current regime cycles reflects changes in charge/discharge profiles in regions corresponding to hydrogen sorption-desorption process. No distortion at 0.5–0 V and no sharp change of the curve slope in the region of 0–0.2 V might suggest that the hydrogen sorption/desorption reaction was suppressed by increased iodine/iodide redox activity. Finally, both these experiments confirmed high voltage stability of hybrid electrolyte system.

3.4. Self-discharge phenomena

The profile of self-discharge vs. time and vs. log(t) during 20 h of open circuit voltage is presented in Fig. 7.

During first 5 hours at open circuit conditions, the initial voltage has declined by 40%. Afterwards, the voltage is stabilized and after next 5 h the voltage dropped below 50% of initial value. The self-discharge might be attributed to three phenomena: overcharging and electrolyte decomposition (non-diffusion controlled), redox activity due to impurities and redox active species (diffusion controlled), and ohmic 'leak' associated with construction failure. The self-discharge mechanism involving faradaic process is represented as a linear dependence of the voltage versus log(t). Since the maximum cell voltage is higher than water decomposition voltage, one may expect discharging effects of this phenomenon. However, there is no linear fit at the beginning of the self-discharge curve. Nevertheless, after 5 h at open circuit conditions the linear fitting of the self-discharge profile on the log(t) scale is obtained and may correspond to redox activity of electrolyte [44–47]. Based on Fig. 3 one may conclude that after reaching 1 V of the cell

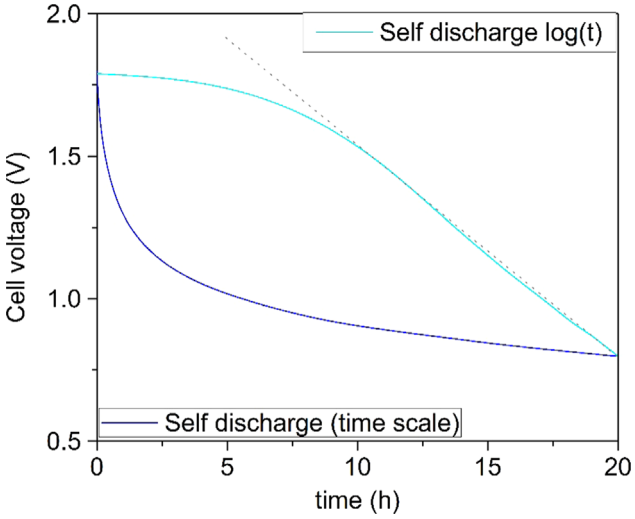

Fig. 7. Profile of self-discharge vs. time and vs. log(t) during 20 h of open circuit voltage.

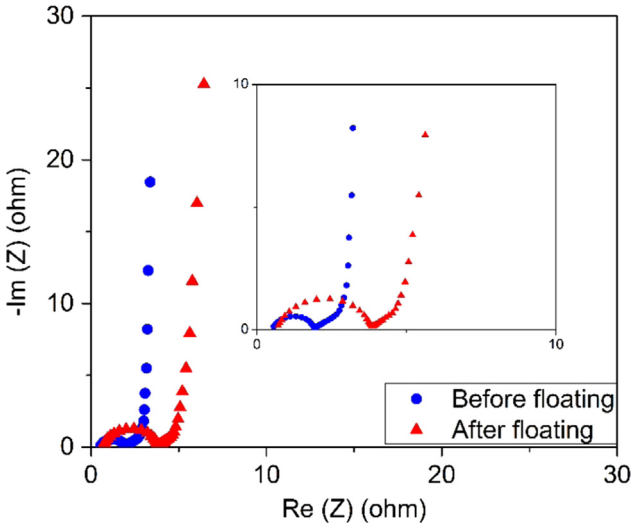

Fig. 8. Nyquist plots of the hybrid device before and after floating test.

voltage, the negative electrode is working above the potential of hydrogen evolution. It might suggest that the initial loss of voltage might be caused by high ionic concentration in the electrode bulk since the charge is stored not only in double-layer but also by weak chemical bonding of nascent hydrogen. After the initial loss of voltage, the stabilization of self-discharge process is connected with iodide/iodine redox activity, confirmed by linear profile on U-log(t) curve. We assume that adsorption of redox species (iodine and hydrogen) and the strength of their bonding with carbon can play important role in self-discharge phenomena. The stronger bonding of species, the lower self-discharge [47].

3.5. Electrochemical impedance spectroscopy

Fig. 8. shows Nyquist plot that represents the results obtained by electrochemical impedance spectroscopy before and after floating test.

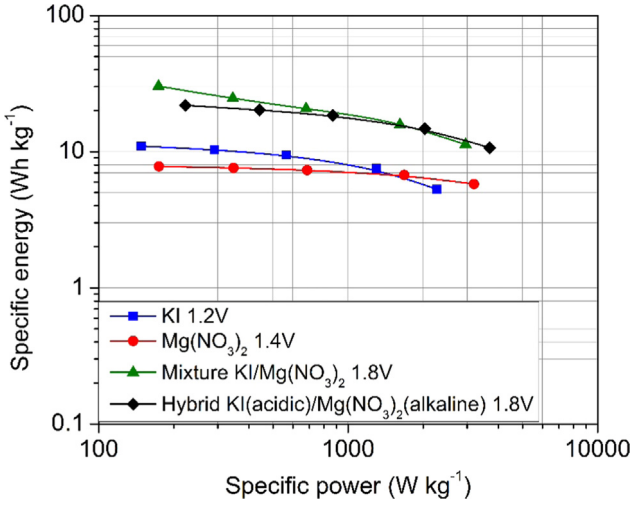

Fig. 9. Ragone plot of capacitors for hybrid, mixture and symmetric electrolytic systems.

The origin of the semi-circle at high frequencies is connected rather with the construction of the cell; electrodes in the form of self-standing pellets may have a limited contact with the current collector and result in significant charge transfer resistance (equivalent distributed resistance). The resistances in the form of the Nyquist plots recorded for the system after and before floating are similar; after 60 hours of floating, equivalent series resistance slightly increased from 0.58 Ω to 0.83 Ω. No visible traces of corrosion led to the conclusion that long-term floating test aggravates rather the electrode material and causes a decrease in conductivity between the electrode and the current collector. We assume that this is reflected in the Nyquist plot as an increase of charge transfer resistance. It suggests that no electronic change occurs in the system. Nevertheless, in both cases the capacitive behavior of the system is well preserved.

3.6. Power and energy performance

Fig. 9 shows Ragone plot obtained for hybrid, mixture, and symmetric systems. Calculation of specific power and specific energy of presented systems was based on galvanostatic charging/discharging method at 0.5–10 A g^{-1} current loads taking into account active material mass of both electrodes. As expected, the hybrid and mixed systems are characterized by energy density twice higher than other presented solutions. Mixed electrolyte system provided the best energy performance; it is however discarded because of low cycle stability.

The hybrid electrolytic system, especially with controlled pH, is characterized by the best power performance. High energy density makes the hybrid electrolyte system an attractive competitor versus existing organic solutions reaching similar energy densities.

4. Conclusions

The high-voltage capacitor with hybrid aqueous electrolyte was successfully designed, constructed and characterized. A

variety of performed experiments proved the superiority of electrolyte hybridization. We confirmed that a good separation of electrolytes plays a crucial role for the voltage enhancement; electrodes operating in electrolyte with various pH demonstrated a significant shift for hydrogen and oxygen evolution potentials. Moreover, the negative electrode operates near to hydrogen evolution potentials and boosts the capacitance from pseudocapacitive effect of hydrogen storage while redox activity of iodide/iodine redox couple preserves the positive electrode against oxidation. Long-term cycling as well as floating tests confirmed the stability of the system. Finally, the proposed design allows us to overcome the water decomposition and to reach 1.8 V capacitor voltage. The energy density of 20 W h/kg has been achieved at 1 kW/kg power rate.

Acknowledgments

The authors gratefully acknowledge the Polish-Swiss Research Programme, Project no. PSPB 107/2010 (INGEC) and Ministry for Science and Higher Education (DS-PB 31-295/2015) for financial support.

References

[1] H.E. Becker, Low voltage electrolytic capacitor, US Patent 2 800 616 to General Electric, 1957.
[2] D.I. Boos, Electrolytic capacitor having carbon paste electrodes, US Patent 3 536 963 to Standard Oil, SO-HIO, 1970.
[3] H.Y. Lee, J.B. Goodenough, Supercapacitor behavior with KCl electrolyte, J. Solid State Chem. 144 (1999) 220–223.
[4] J. Jiang, A. Kucernak, Electrochemical supercapacitor material based on manganese oxide: preparation and characterization, Electrochim. Acta 47 (2002) 2381–2386.
[5] T. Brousse, M. Toupin, D. Bélanger, A hybrid activated carbon-manganese dioxide capacitor using a mild aqueous electrolyte, J. Electrochem. Soc. 151 (2004) A614–A622.
[6] G. Lota, K. Fic, E. Frackowiak, Carbon nanotubes and their composites in electrochemical applications, Energy Environ. Sci. 4 (2011) 1592–1605.
[7] J. Whitacre, D. Humphreys, W. Yang, E. Lynch-Bell, A. Mohammad, E. Weber, D. Blackwood, Aqueous electrolyte energy storage device US Patent 8 298 701 to Aquion Energy Inc., 2012.
[8] K. Fic, G. Lota, M. Meller, E. Frackowiak, Novel insight into neutral medium as electrolyte for high-voltage supercapacitors, Energy Environ. Sci. 5 (2012) 5842–5850.
[9] T. Morimoto, K. Hiratsuka, Y. Sanada, H. Aruga, Electric double-layer capacitor US Patent 4 725 927 to Asahi Glass Co. and Elna Co. Ltd., 1988.
[10] J. Tabuchi, T. Saito, A. Ochi, Y. Shimizu, Activated carbon/polyacene composite and process for producing the same US Patent 5 172 307 to NEC Corp., 1992.
[11] A. Yoshida, K. Imoto, Electric double-layer capacitor and method for producing the same US Patent 5 150 283 to Matsushita Electric Industrial Co. Ltd., 1992.
[12] J.C. Farahmendi, J.M. Dispennette, E. Blank, A.C. Kolb, Multi-electrode double-layer capacitor WO9815962 to Maxwell Technologies, 1998.
[13] C. Wei, E.C. Jarabek, O.H. Leblanc Jr, Ultracapacitor separator WO0019464 to General Electric Co., 2001.
[14] C. Arbizzani, M. Biso, M. Lazzari, F. Soavi, M. Mastragostino, Safe, high-energy supercapacitors based on solvent-free ionic liquid electrolytes, J. Power Sources 185 (2008) 1575–1579.
[15] A. Balducci, F. Soavi, M. Mastragostino, The use of ionic liquids as solvent-free green electrolytes for hybrid supercapacitors, Appl. Phys. A 82 (2006) 627–632.
[16] F. Béguin, E. Frackowiak, Supercapacitors Materials, Systems, and Applications, Wiley-VCH, Germany, 2013.
[17] T. Brousse, D. Bélanger, J.W. Long, To be or not to be pseudocapacitive?, J. Electrochem. Soc. 162 (2015) A5185–A5189.
[18] B.E. Conway, Electrochemical Supercapacitors: Scientific fundamentals and Technological Applications, Springer Science, New York, 1999.
[19] R. Kötz, M. Carlen, Principles and applications of electrochemical capacitors, Electrochim. Acta 45 (2000) 2483–2498.
[20] P. Verma, P. Maire, P. Novák, A review of the features and analyses of the solid electrolyte interphase in Li-ion batteries, Electrochim. Acta 55 (2010) 6332–6341.
[21] C. Decaux, G. Lota, E. Raymundo-Pinero, E. Frąckowiak, F. Béguin, Electrochemical performance of a hybrid lithium-ion capacitor with a graphite anode preloaded from lithium bis(trifluoromethane)sulfonimide-based electrolyte, Electrochim. Acta 86 (2012) 282–286.
[22] N. Ogihara, Y. Igarashi, A. Kamakura, K. Naoi, Y. Kusachi, K. Utsugi, Disordered carbon negative electrode for electrochemical capacitors and high-rate batteries, Electrochim. Acta 51 (2006) 1713–1720.
[23] K. Naoi, S. Ishimoto, J. Miyamoto, W. Naoi, Second generation 'nanohybrid supercapacitor': evolution of capacitive energy storage devices, Energy Environ. Sci. 5 (2012) 9363–9373.
[24] G. Lota, K. Fic, E. Frackowiak, Alkali metal iodide/carbon interface as a source of pseudocapacitance, Electrochem. Commun. 13 (2011) 38–41.
[25] K. Fic, M. Meller, E. Frackowiak, Interfacial redox phenomena for enhanced aqueous supercapacitors, J. Electrochem. Soc. 162 (2015) A5140–A5147.
[26] A. Burke, Ultracapacitors: why, how, and where is the technology, J. Power Sources 9 (2000) 37–50.
[27] V. Khomenko, E. Raymundo-Pinero, F. Béguin, High-energy density graphite/AC capacitor in organic electrolyte, J. Power Sources 177 (2008) 643–651.
[28] P. Ratajczak, K. Jurewicz, P. Skowron, Q. Abbas, F. Béguin, Effect of accelerated ageing on the performance of high voltage carbon/carbon electrochemical capacitors in salt aqueous electrolyte, Electrochim. Acta 130 (2014) 344–350.
[29] C. Hsu, C. Hu, Synthesis and characterization of mesoporous spinel $NiCo_2O_4$ using surfactant-assembled dispersion for asymmetric supercapacitors, J. Power Sources 242 (2013) 662–671.
[30] H. Hsu, K. Chang, R.R. Salunkhe, C. Hsu, C. Hu, Synthesis and characterization of mesoporous Ni–Co oxy-hydroxides for pseudocapacitor application, Electrochim. Acta 94 (2013) 104–112.
[31] T. Ou, C. Hsu, C. Hu, Synthesis and characterization of sodium-doped MnO_2 for the aqueous asymmetric supercapacitor application, J. Electrochem. Soc. 162 (2015) A5124–A5132.
[32] G. Lota, E. Frackowiak, Striking capacitance of carbon/iodide interface, Electrochem. Commun. 11 (2009) 87–90.
[33] K. Fic, M. Meller, E. Frackowiak, Strategies for enhancing the performance of carbon/carbon supercapacitors in aqueous electrolytes, Electrochim. Acta 128 (2014) 210–217.
[34] S. Roldan, M. Granda, R. Menendez, R. Santamaria, C. Blanco, Mechanisms of energy storage in carbon-based supercapacitors modified with a quinoid redox-active electrolyte, J. Phys. Chem. C. 115 (2011) 17606–17611.
[35] E. Frackowiak, M. Meller, J. Menzel, D. Gastol, K. Fic, Redox-active electrolyte for supercapacitor application, Faraday Discuss. 172 (2014) 179–198.
[36] Q. Li, K. Li, C. Sun, Y. Li, An investigation of Cu^{2+} and Fe^{2+} ions as active materials for electrochemical redox supercapacitors, J. Electroanal. Chem. 611 (2007) 43–50.
[37] E. Frackowiak, K. Fic, M. Meller, G. Lota, Electrochemistry serving people and nature: High-energy ecocapacitors based on redox-active electrolytes, ChemSusChem 5 (2012) 1181–1185.
[38] K. Babel, D. Janasiak, K. Jurewicz, Electrochemical hydrogen storage in activated carbons with different pore structures derived from certain lignocellulose materials, Carbon 50 (2012) 5017–5026.
[39] F. Béguin, M. Friebe, K. Jurewicz, C. Vix-Guterl, J. Dentzer, E. Frackowiak, State of hydrogen electrochemically stored using

nanoporous carbons as negative electrode materials in an aqueous medium, Carbon 44 (2006) 2392–2398.
[40] K. Jurewicz, E. Frackowiak, F. Béguin, Nanoporous H-sorbed carbon as anode of secondary cell, J. Power Sources 188 (2009) 617–620.
[41] F. Béguin, K. Kierzek, M. Friebe, A. Jankowska, J. Machnikowski, K. Jurewicz, E. Frackowiak, Effect of various porous nanotextures on the reversible electrochemical sorption of hydrogen in activated carbons, Electrochim. Acta 51 (2006) 2161–2167.
[42] K. Babel, K. Jurewicz, KOH activated lignin based nanostructured carbon exhibiting high hydrogen electrosorption, Carbon 46 (2008) 1948–1956.
[43] D. Weingarth, A. Foelske-Schmitz, R. Kötz, Cycle versus voltage hold – Which is the better stability test for electrochemical double-layer capacitors?, J. Power Sources 225 (2013) 84–88.
[44] B.E. Conway, W.G. Peel, T.C. Liu, Diagnostic analyses for mechanisms of self-discharge of electrochemical capacitors and batteries, J. Power Sources 65 (1997) 53–59.
[45] B.W. Ricketts, C. Ton-That, Self-discharge of carbon-based supercapacitors with organic electrolytes, J. Power Sources 89 (2000) 64–69.
[46] H.A. Andreas, Self-discharge in electrochemical capacitors: a perspective article, J. Electrochem. Soc. 162 (2015) A5047–A5053.
[47] S. Chun, B. Evanko, X. Wang, D. Vonlanthen, X. Ji, G.D. Stucky, S. W. Boettcher, Design of aqueous redox-enhanced electrochemical capacitors with high specific energies and slow self-discharge, Nat. Commun. 6 (2015) 7818.